Available online at www.sciencedirect.com
ScienceDirect
Journal of Colloid and Interface Science 321 (2008) 484–492
JOURNAL OF Colloid and Interface Science
www.elsevier.com/locate/jcis

Synthesis of cobalt ferrite core/metallic shell nanoparticles for the development of a specific PNA/DNA biosensor

Marcos Pita [a,*], José María Abad [b], Cristina Vaz-Dominguez [a], Carlos Briones [c], Eva Mateo-Martí [c], José Angel Martín-Gago [c,d], Maria del Puerto Morales [d], Víctor M. Fernández [a]

[a] *Instituto de Catálisis y Petroleoquímica, CSIC, C/Marie Curie 2, 28049 Cantoblanco, Madrid, Spain*
[b] *University of Liverpool, Department of Chemistry, Liverpool L69 7ZD, United Kingdom*
[c] *Centro de Astrobiología (CSIC-INTA), Carretera de Ajalvir Km 4, 28850 Torrejón, Madrid, Spain*
[d] *Instituto de Ciencia de Materiales de Madrid, CSIC, C/Sor Juana Inés de la Cruz 3, 28049 Cantoblanco, Madrid, Spain*

Received 25 January 2008; accepted 6 February 2008

Available online 13 February 2008

Abstract

Controlled synthesis of cobalt ferrite superparamagnetic nanoparticles covered with a gold shell has been achieved by an affinity and trap strategy. Magnetic nanoparticles are functionalized with a mixture of amino and thiol groups that facilitate the electrostatic attraction and further chemisorption of gold nanoparticles, respectively. Using these nanoparticles as seeds, a complete coating shell is achieved by gold salt-iterative reduction leading to monodisperse water-soluble gold-covered magnetic nanoparticles, with an average diameter ranging from 21 to 29 nm. These constitute a versatile platform for immobilization of biomolecules *via* thiol chemistry, which is exemplified by the immobilization of peptide nucleic acid (PNA) oligomers that specifically hybridize with complementary DNA molecules in solution. Hybridation with DNA probes has been measured using Rhodamine 6G fluorescence marker and the detection of a single nucleotide mutation has been achieved. These results suggest the PNA-nanoparticles application as a biosensor for DNA genotyping avoiding commonly time-consuming procedures employed.

Keywords: Magnetic nanoparticle; Gold shell; Peptide nucleic acid; DNA–PNA hybridization; Mutation detection; Rhodamine 6G

1. Introduction

In recent years, the synthesis of composite magnetic nanomaterials has received increasing attention due to their electronic, magnetic, catalytic and chemical or biological sensing properties [1]. Currently, magnetic nanoparticles offer widespread applications in biotechnology, such as deoxyribonucleic (DNA) and ribonucleic (RNA) acid purification [2], cell separation, drug delivery, magnetic resonance imaging [3] and hyperthermia cancer treatments [4,5]. In this sense, magnetic nanoparticles show high magnetic susceptibility and good dispersibility, however resistance to oxidation and stability in physiological environments are also required [5]. Covering magnetic nanoparticles with an external inert shell such as gold has been attempted in order to add new properties (inertness, protection of the magnetic core against oxidation) to those of the particles, without modifying their superparamagnetic behavior [6–8]. Moreover, gold allows a number of possibilities for detection and provides an optimized platform for chemical functionalization through the attachment of thiolated molecules, which form self-assembled monolayers (SAMs). Therefore, surface-modified nanoparticles constitute a fully functional material that can be used either as an *in vivo* probe or as a nanostructured biosensor [9]. Although magnetic and metallic nanoparticles have been widely investigated [10,11], few works have been published on the development of a combined approach to achieve this composite material [12–15]. Some methods commonly used for obtaining metal oxide core/Au shell magnetic nanoparticles are based on a reversed micelle system. These systems are less suitable for biological applications due to the use of harmful surfactants or organic solvents [16–18]. Recently, a water-based synthesis method involving ultravio-

* Corresponding author. Fax: +34 915854760.
E-mail address: marcospita@icp.csic.es (M. Pita).

0021-9797/$ – see front matter
doi:10.1016/j.jcis.2008.02.010

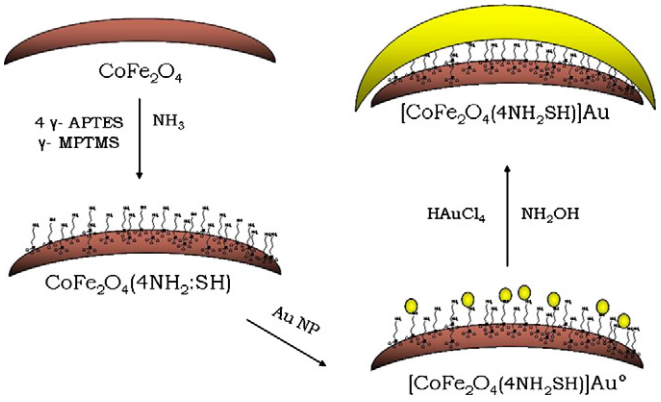

Scheme 1. Reaction strategy showing the successive steps for gold covering process onto 4:1 amino:mercapto functionalized cobalt ferrite nanoparticles.

let (UV) radiation was used to cover iron oxide/titanium oxide nanoparticles with gold [11], however it yielded incomplete gold coverage and required several complicated steps.

Here we describe the synthesis of water-soluble gold-covered magnetic nanoparticles as well as their use for the development of specific DNA biosensors. One of the present work aims has been the optimization of the metallic covering stage which was achieved by bonding gold seeds through an affinity and trap strategy (Scheme 1). Magnetic nanoparticles are functionalized with a mixture of amino and thiol groups that facilitate the electrostatic attraction and further chemisorption of the gold nanoparticles, respectively. Using these gold nanoparticles as seeds, a complete coating shell is achieved by gold salt-iterative reduction [19].

Thiol-modified single stranded peptide nucleic acid (ssPNA) oligomers can be directly immobilized onto Au-magnetic nanoparticles following a procedure previously optimized for the formation of PNA SAMs on gold surfaces [20]. These PNA-modified, gold-covered magnetic nanoparticles can interact specifically with a DNA target molecule complementary to the attached PNA probe (Scheme 2). The specific PNA–DNA hybridization is monitored by the detection of an external fluorescent molecule, Rhodamine 6G, which intercalates in the PNA–DNA double helix and also associates electrostatically to the phosphate groups present in the DNA backbone [21].

2. Experimental

2.1. Materials

All chemicals were used as purchased. $CoCl_2{\cdot}6H_2O$, $FeCl_3{\cdot}6H_2O$, $Fe(NO_3)_3{\cdot}9H_2O$, γ-aminopropyltriethoxysilane (APTES), γ-mercaptopropyltrimethoxysilane (MPTMS) and $HAuCl_4$ were acquired from Sigma with ACS Reagent purity grade. Tetrakis (hydroxymethyl)phosphonium chloride (THPC) and hydroxylamine hydrochloride ($NH_2OH{\cdot}HCl$) were purchased to Fluka. The ssPNA molecule used was supplied by Isogen Life Science. It contained a sequence of 11 nucleotides (nt) complementary to a characteristic region of one of the proteins that constitute the capsid of the foot-and-mouth disease virus (FMDV). The PNA sequence is: Cys-O-O-AATCCCCGGAT where each of the two "O" spacer units is a 1.5 nm long molecule of 8-amino-3,6-dioxaoctanoic acid, and the amino acid cysteine (Cys) that provides the terminal thiol group to the PNA molecule that allows further chemisorption on a gold surface. ssDNA oligomers containing the fully complementary sequence (5′-ATCCGGGGATT-3′) (HIBR), or with an oligomer identical in all positions but the central one, with a single nucleotide mutation (5′-ATCCGAGGATT-3′) (SMM) were purchased to Isogen Life Science.

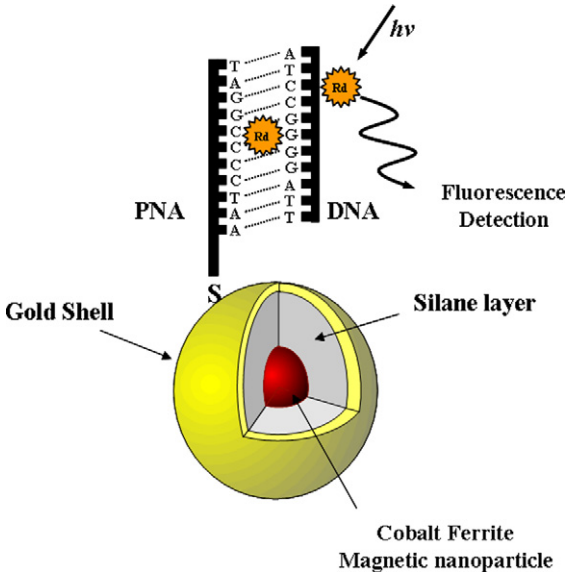

Scheme 2. Functionalized gold shell–cobalt ferrite nanoparticles with thiolated PNA for hybridation with complementary DNA target molecules and further fluorescence detection by intercalated or electrostatically associated Rhodamine 6G.

2.2. Synthesis of cobalt ferrite magnetic nanoparticles

The cobalt ferrite synthesis was carried out according to previous work [22–24]. 5 mL of 2 M $CoCl_2{\cdot}6H_2O$ (Sigma, ACS reagent) in HCl 7.4% solution and 40 mL of 0.5 M $FeCl_3{\cdot}6H_2O$ in Milli Q water were pre-heated to 50 °C, mixed and poured into a boiling solution of 200 mL 1 M NaOH under vigorous stirring. The boiling was maintained for 30 min and the solution was cooled down to room temperature without stirring. After five water-cleaning stages by magnetic sedimenting and decanting of supernatant, the ferrofluid was treated with an oxidative reaction to passivate the surface by redispersion in 30 mL of 2 M HNO_3 solution containing 0.35 M $Fe(NO_3)_3{\cdot}9H_2O$ and heating to 100 °C for 45 min under continuous stirring. The resulting product was magnetically sedimented overnight. Finally, the supernatant was decanted and substituted by 100 mL of Milli Q water.

2.3. Functionalization of magnetic nanoparticles with amine and thiol groups

The reaction was carried out at room temperature by mixing in a round-bottomed flask 288 mL of absolute ethanol, 2 mL of the cobalt-ferrite ferrofluid ($\approx$16 mg mL^{-1}) and 12 mL of 30%

NH_3 solution, according to Ref. [24]. The silane reactant mixture was added up to a final concentration of 0.5%. Two silane coupling agents were employed, APTES and MPTMS, which append amino and thiol functional groups to the magnetic nanoparticles, respectively. The proportion was varied in order to optimize the colloidal stability. Silane modified nanoparticles are named as [M_2(NH_2:SH)].

2.4. Synthesis and attachment of gold nanoparticles (AuNPs) on M_2(NH_2:SH) magnetic nanoparticles

Gold nanoparticles were freshly synthesized in aqueous media by the reduction of 1 mM $HAuCl_4$ in 60 mM NaOH solution with 1 mM THPC [25]. This reducing agent was added to the alkaline solution followed by the $HAuCl_4$ solution under a vigorous stirring. The resulting nanoparticles were filtered with a PTFE 0.200 μm pore size filter. A dispersion of these AuNPs (10 mL, 80 nM of particles) was reacted with 10 mL of [M_2(NH_2:SH)] magnetic nanoparticles (3 mg mL^{-1}) in order to achieve the attachment of gold seeds on the magnetic nanoparticle functionalized surface. The gold-seed magnetic nanoparticles obtained [M_2(NH_2:SH)Au°] were separated by magnetic attraction and extensively rinsing.

2.5. Formation of a gold shell onto M_2(NH_2:SH)Au° magnetic nanoparticles

The gold shell was achieved following a previous procedure which was slightly modified [24,26]. 1 mL of the solution containing 3 mg mL^{-1} of M_2(NH_2:SH)Au° nanoparticles were diluted ten times with Milli Q water, followed by 10 μL of 2.5 mM $HAuCl_4$ under vigorous stirring. Reduction was carried out by adding 30 μL of a freshly prepared 5 mM $NH_2OH{\cdot}HCl$ solution [21]. After the gold salt reduction, the nanoparticles were magnetically sedimented, washed and decanted twice with 1 mL of water to remove reaction byproducts. This procedure was repeated up to six times in order to achieve a complete shell covering. Particles coated with Au will be named as M_2($4NH_2$–SH)Au.

2.6. Immobilization of PNA on gold-covered magnetic nanoparticles

The ssPNA immobilization was carried out by adding 4 μL of 100 μM thiolated PNA to 96 μL of M_2($4NH_2$–SH)Au nanoparticles with a concentration of 0.3 mg mL^{-1}, getting a final PNA concentration of 4 μM. This mixture was incubated for 190 min at 23 °C, and the particles were then sedimented magnetically for 20 min. The supernatant was replaced by 100 μL of a 1 mM 6-mercapto-1-hexanol solution and left to react for 60 min in order to achieve a blockage of the remained Au surface. The PNA-modified nanoparticles [M_2($4NH_2$–SH)Au–PNA] were separated by magnetic sedimentation and washed twice with 1 mM HEPES buffer pH 7.5.

2.7. Hybridization experiments

Hybridization experiments were carried out incubating M_2($4NH_2$–SH)Au–PNA nanoparticles with the HIBR or the SMM ssDNA probe. PNA-modified nanoparticles were resuspended in 1 mM HEPES buffer pH 7.5 and DNA target molecules were added to a final concentration of 4 μM. The reaction was performed for 60 min at 40 °C. Afterwards, nanoparticles were separated by magnetic sedimentation and washed three times with a solution containing 4 mM sodium citrate and 40 mM NaCl pH 7, at a temperature ranged from 45 to 47 °C to remove non-specific DNA hybridizations. The magnetic sedimentation washing procedure was repeated twice, followed by three washing steps with water. Rhodamine 6G was added to a 10 μM final concentration and incubated for 30 min. Then the nanoparticles were sedimented magnetically, the supernatant was replaced with water. This procedure was repeated three times, and the remaining fluorescence was measured.

2.8. Characterization techniques

The phases present in the nanoparticle samples were identified by powder X-ray diffraction measurements using a Seifert XRD 3000P and Cu$K\alpha$ radiation. The crystalline size was calculated from the full width at half maximum of the highest reflection using the Scherrer's equation [27].

The morphology and the particle size distribution were investigated using a transmission electron microscope (TEM) (JEOL-2000 FXII). The sample preparation was carried out by immersion of the nanoparticles dispersion in an ultrasonic bath for one hour and then a drop of this solution was deposited onto a carbon mesh on a copper grid. In all cases, the average particle length and the standard deviation were calculated by counting around 200 particles.

Colloidal properties of the samples were studied in a Zeta Sizer Nano S (Malvern). The electrophoretic mobility was measured as a function of pH at 25 °C, using KNO_3 as electrolyte and HNO_3 and KOH to adjust the pH of the suspensions. Dynamic light scattering measurement of gold-covered magnetic nanoparticles was carried on a Particle Size Analyzer 90 Plus (Brookhaven Instruments Corporation, NY, USA).

Plasmon resonance was measured with an UV–vis spectrometer Uvikon 945. The absorption range was from 750 to 300 nm.

The experimental set-up for XPS measurements consists of an ultra high vacuum (UHV) chamber equipped with a hemispherical electron analyzer, and a X-ray source operated by using Mg$K\alpha$ radiation (1253.6 eV). The base pressure in the ultra high vacuum chamber was 1×10^{-9} mbar, and the measurements were carried out at room temperature. The pass energy applied for taking the overview sample was 30 eV, while 20 eV pass energy was applied for the fine analysis of the core level spectra. The binding energies were calibrated against the binding energy of the C 1s peak at 285.0 eV (attributed to hydrocarbon contamination, this reference gave binding energy values accurate to within ±0.1 eV). XPS measurements of particles were carried out by obtaining a solid pellet mixing the nanopar-

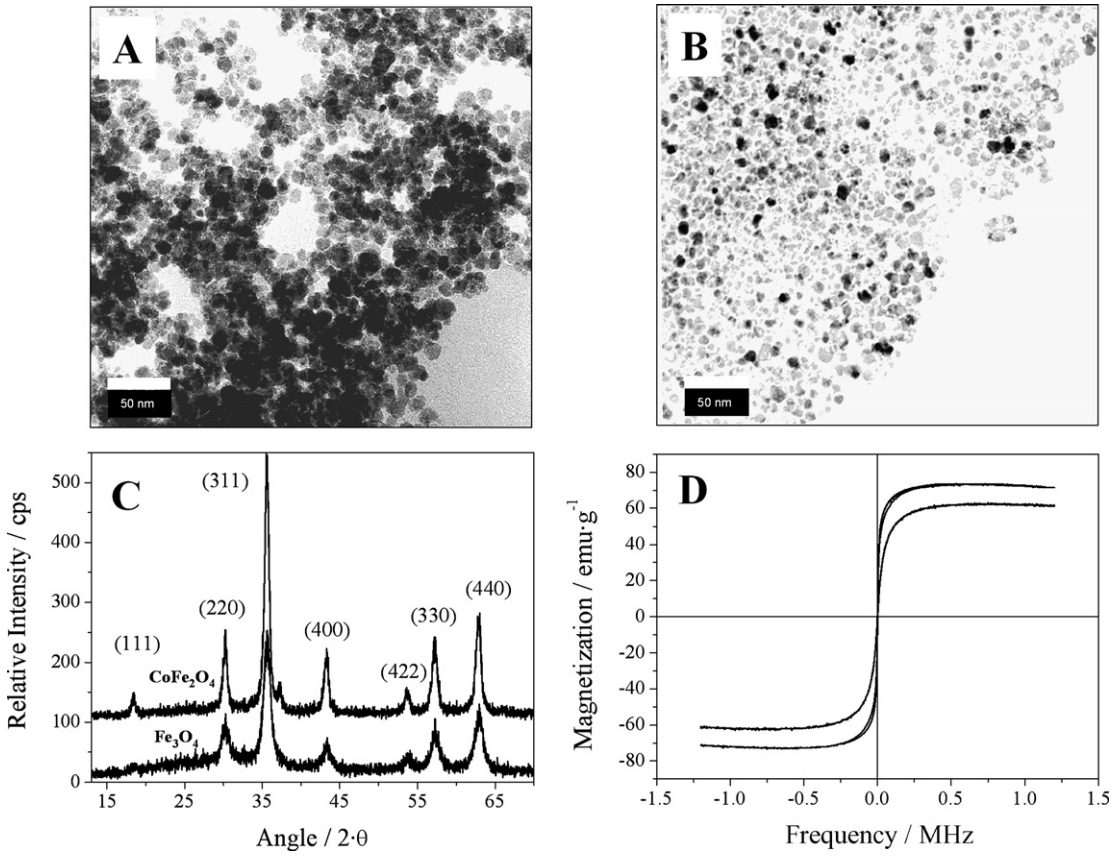

Fig. 1. Characterization of the different ferrofluids: TEM micrographs (bar represents 100 nm) of cobalt ferrite (A) and magnetite (B). (C) X-ray diffraction patterns for cobalt ferrite and magnetite. (D) Magnetization curves for cobalt ferrite and magnetite.

ticles with a KBr solvent, and then the powder was pressed to make a compacted sample. XPS spectrum of the pellet without nanoparticles was recorded to identify the presence of elements coming from the solvent that could be erroneously assigned to species from the nanoparticles.

Magnetic characterization of the samples was carried out in a vibrating sample magnetometer (MLVSM9 MagLab 9 T, Oxford Instrument) at room temperature. Magnetization curves were recorded by first saturating the sample in a field of 5 T; then, the saturation magnetization (Ms), and the coercive field (Hc) were determined for each sample.

Fluorescent measurements were performed with a Luminescence Spectrometer Perkin Elmer LS50B device. The configuration for the fluorescence measurements was 15.0 slits width for the entrance and 5.0 slits for the detection. The excitation wavelength for Rhodamine 6G was set at 528 nm, and the emission wavelength was set at 545 nm.

The infrared spectra were recorded with a Nicolet 860 Fourier transform spectrometer equipped with an magnesium–calcium–tellurium (MCT) detector and a purge gas system for removal of CO_2 and H_2O (Whatman) in transmission mode. The IR spectra were averaged over 1024 scans; the spectral resolution was 2 cm^{-1}. The spectra were blank subtracted and baseline corrected using OMNIC software from Nicolet. The sample was prepared by evaporation to dryness of the PNA-modified nanoparticles on a polished BaF_2 window.

3. Results and discussion

3.1. Magnetic core synthesis

Cobalt ferrite nanoparticles were synthesized by coprecipitation of Fe(III) and Co(II) salts [19] as described in Section 2. TEM characterization (Fig. 1A) shows that the cobalt ferrite cores have an average diameter of 18 ± 3 nm. This is in good agreement with a crystal size of 17 nm obtained by XRD from diffraction pattern (Fig. 1C) using Scherrer's equation [27]. This X-ray pattern corresponds to a well-crystallized inverse spinel structure. Stability of the colloid at the pH values required for further modification is a crucial feature of the functionalization strategy. Therefore the isoelectric point (pI) of the ferrofluid, was obtained by measuring the electrophoretic mobility as a function of the pH resulting in a value of 7.5. The properties of the cobalt ferrite ferrofluid were compared with a magnetite ferrofluid synthesized by Massart's method [23], i.e. by coprecipitation of Fe(II) and Fe(III) salts. It yielded nanoparticles with a mean size of 11 ± 2 nm as observed by TEM (Fig. 1B), and a crystal size of 10 nm with an inverse spinel structure obtained by XRD (Fig. 1C).

A pI of 8.2 was obtained for this ferrofluid which revealed that the cobalt ferrite is more suitable for further modification with silane-coupling agents rather than magnetite which pH of 9.5 causes flocculation. Moreover, magnetization stud-

ies (Fig. 1D) reported values of magnetization at saturation (Ms) slightly higher for cobalt ferrite (67 emu g^{-1}) than for magnetite (62 emu g^{-1}) at room temperature and a significant higher susceptibility, which means that saturation is attained at a lower magnetic field for cobalt ferrite particles.

3.2. Functionalization of magnetic nanoparticles with thiol and amine groups

The functionalization of cobalt ferrite magnetic nanoparticles was based on a silane condensation reaction between cobalt ferrite hydroxyl surface groups and amine (APTES) and thiol (MPTMS) silane coupling agents [24]. The particles were capped with a mixed APTES:MPTMS layer by reaction with different molar ratios in solution. Functionalized nanoparticles with only APTES showed a high stability in solution due to the electrostatic repulsions between protonated amine groups. On the contrary, nanoparticles functionalized with only MPTMS or molar ratios of 1:1, 2:1, 3:1 APTES, MPTMS resulted in aggregation yielding an amorphous silica micron-size matrix with embedded magnetic nanoparticles (see Fig. S1 in Supporting information) due to a lack of electrostatic repulsion. A 4:1 ratio [M_2(4NH_2:SH)] provided optimal stability in aqueous media and sufficient coverage (*vide infra*) with amino groups and thiol groups for electrostatic affinity and for covalent attachment of gold seeds.

3.3. Attachment of gold seeds

The formation of a gold shell onto functionalized M_2(NH_2:SH) magnetic nanoparticles was carried out by the attachment of gold nanoparticles (AuNPs) as seeds for a further metallic growth step. Functionalized magnetic nanoparticles were reacted with AuNPs of 4 ± 2 nm diameter prepared in aqueous media using Duff's method [25].

Magnetic nanoparticles only modified with amine groups M_2(NH_2) showed an electrostatic attraction with the negatively charged AuNPs surface. However, this binding was dependent on the pH and ionic strength of the solution and the attached AuNPs were released when the pH was increased to alkaline values. To overcome this instability a mixed layer [M_2(4NH_2:SH)] with terminal thiol and amino groups were used to covalently attach the electrostatic attracted AuNPs to the magnetic nanoparticles.

The reaction was carried out at low pHs to favor electrostatic interactions and increase the immobilization rate by induced proximity effect between thiol groups and gold surface from adsorbed AuNPs. Fig. 2 shows the surface plasmon band (SPB) of the AuNPs that remained attached to M_2(4NH_2:SH) magnetic nanoparticles after 1 h of reaction at pHs 4 and 6.5 and subsequent increment to pH 11. 71% of the initial SPB (Fig. 2b) was retained on the modified nanoparticles after magnetic attraction and rinsing when the immobilization was performed at pH 4 (Fig. 2a), whereas only 50% of the SPB was observed (Fig. 2c) when the reaction was carried out at pH 6.5. In both cases a shift, as well as a broadening of the gold SPB is observed due to the AuNPs attachment onto the magnetic particles.

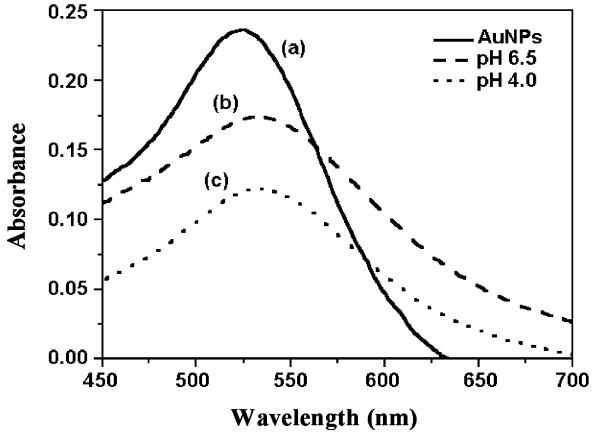

Fig. 2. Increase of the plasmon resonance absorption band from the gold shell that remains attached to the magnetic nanoparticles. (a) Solid line: gold nanoparticles. (b) Dashed line: M_2(4NH_2–SH)Au° when the gold attachment pH was decreased to 4. (c) Dotted line: M_2(4NH_2–SH)Au° when the pH for the gold attachment step was lowed to 6.5.

The requirement of the simultaneous presence of thiol and amino groups in the layer to obtain stable gold attachment is also illustrated by the measurement of the amount of AuNPs released at alkaline pH. At alkaline pH the amino groups on magnetic particles deprotonate, releasing the electrostatic attracted AuNP. Fig. 3 shows supernatant UV–vis spectra of AuNPs incubated with M_2(4NH_2:SH) (Fig. 3A) or M_2(NH_2) (Fig. 3B) particles at pH 5 for 12 h after magnetic attraction. No SPB was observed in the case of M_2(4NH_2:SH) indicated that all AuNPs were attached onto the magnetic nanoparticles.

To ascertain that the AuNPs are covalently attached to the magnetic cores, the magnetic nanoparticles were dispersed at pH 11 by brief sonication, and a small SPB was observed from the AuNPs (Fig. 3A, dashed curve). When a subsequent magnetic sedimentation (Fig. 3A, dotted curve) was performed the supernatant remained transparent, showing that the gold is covalently attached to the magnetic nanoparticles. On the contrary, a SPB from AuNPs was obtained in the supernatant UV–vis spectrum for M_2(NH_2) particles after incubation. When these were dispersed at pH 11 an increase of the SPB was observed from released AuNPs due to the suppression of electrostatic interactions. Moreover, AuNPs remained also in solution after subsequent magnetic attraction of M_2(NH_2) nanoparticles demonstrating that they were electrostatically attached.

These experiments show the highest stability of the gold nanoparticles on the magnetic surface, induced by the use of a mixed layer of amino and thiol groups instead of amino groups only.

3.4. Gold shell covering

Once the AuNPs are covalently attached to the magnetic nuclei [M_2(4NH_2–SH)Au°], a gold layer on the magnetic nanoparticles was formed by iterative reduction of $HAuCl_4$ with hydroxylamine as reducing agent [26]. The process was characterized by UV–visible spectroscopy. Fig. 4 shows the spectra of M2(4NH_2–SH)Au° particles (curve a) and their successive gold growths (curves b–d).

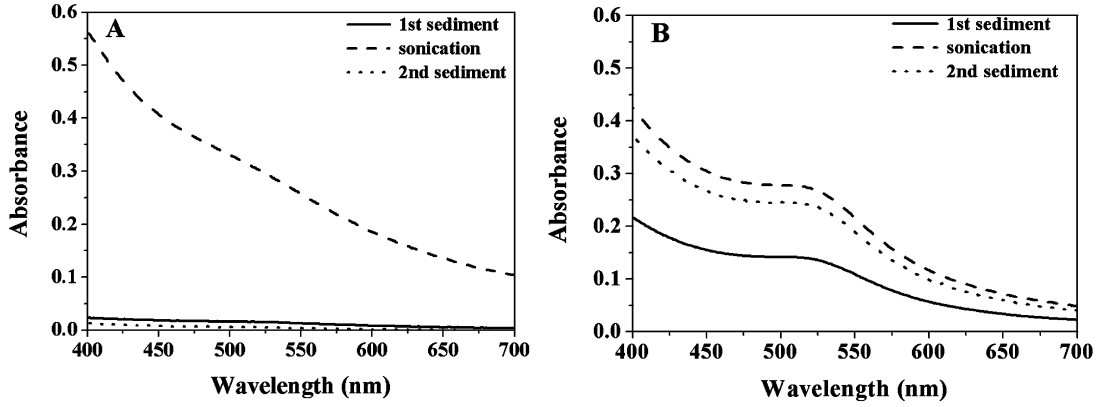

Fig. 3. Gold nanoparticles plasmon band remaining in the supernatant at pH 11. Initial conditions after sedimenting (solid), after ultrasound redispersion (dashed) and second magnetic sedimenting (dotted). (A) Gold immobilized on $M_2(4NH_2–SH)$ functionalized magnetic nanoparticles. (B) Gold immobilized on $M_2(NH_2)$ functionalized magnetic nanoparticles.

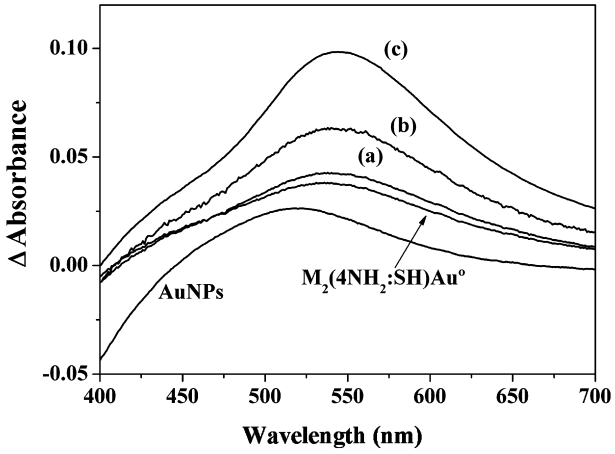

Fig. 4. Evolution of plasmon resonance band when adding iterative gold reduction stages on the M2($4NH_2$–SH)Au° nanoparticles. (a), (b) and (c) curves correspond to 1st, 2nd and 4th reduction stages, respectively.

A surface plasmon band shift to higher wavelengths is observed as consequence of the size increase of the gold layer after every reduction step. It is noteworthy that the gold growth seems to proceed through to the previously attached AuNPs onto magnetic nanoparticles as control experiments carried out with particles without attached AuNPs yielded to both uncovered particles and free AuNPs in solution.

XRD diffraction results for $CoFe_2O_4$ before and after gold covering are shown in Fig. 5A. After the gold coverage, a new diffraction peak was observed at the value $2\theta = 38°$, that matches with Au(111). TEM characterization (Fig. 5B) reported particles with an average diameter of 25 ± 4 nm. Although the gold-covered magnetic nanoparticles were very stable in solution for months, TEM images indicate some aggregation which can be attributed to occur during the drying of the sample on the grid, as previously reported [28]. However, the size measured by dynamic light scattering technique (DLS) in solution, showed a size distribution between 25 and 42 nm, with the maximum at 28 nm. These measurements suggest that particles remain in solution as monomers or dimmers.

3.5. XPS characterization

In order to have additional information of the chemical species that constitute the nanoparticles, every step of the synthesis process was characterized by X-ray photoelectron spectroscopy (XPS) (see Fig. 6). XPS technique provides information about the chemical form of the different constituents of the nanoparticle. For the first sample measured, the synthesis process was stopped just after the formation of the cobalt ferrite core of the nanoparticles ($CoFe_2O_4$).

Fig. 6A shows the core-level spectra of the Fe $2p_{3/2}$ and the Co $2p_{3/2}$. The binding energies of those peaks are 711.4 and 780.4 eV, which correspond to the presence of iron (III) oxide and cobalt (II) oxide respectively. This is coherent with the cobalt ferrite structure, $CoFe_2O_4$. The rest of the analyzed elements (Si, S, N, Au) were absent from the sample. The second sample measured was $M_2(4NH_2–SH)$. In this case the analysis was positive for all the elements tested, except for gold. The oxidation states of silica and oxygen show values that are coherent with the expected structure of the SiO_2. The signals for nitrogen and sulfur atoms show their reduced state, with binding energies of 402.0 and 164.3 eV, respectively. These facts confirm the attachment of APTES and MPTMS to the magnetic core. The third sample analyzed corresponded to the gold capped magnetic particles, $M_2(4NH_2–SH)Au$. In this case the signal of the cobalt and iron oxides, as well as nitrogen and silica, are attenuated. These signals have been screened by the metallic attachment on the nanoparticle surface. The presence of the Au-metallic cover is evidenced in Fig. 6B, where the Au $4f_{5/2}$ core-level peak is clearly observed. The larger peak at 84 eV shown in the figure corresponds to a satellite from the Br 3d coming from the pellet, which has been observed in all the samples, as well as to a contribution of the Au $4f_{7/2}$ in the gold-covered nanoparticles.

3.6. Hybridization of nanoparticle-PNA and DNA: towards a fluorescence-based biosensor

Gold-covered magnetic nanoparticles have been tested as an optimized platform for the attachment of biological macro-

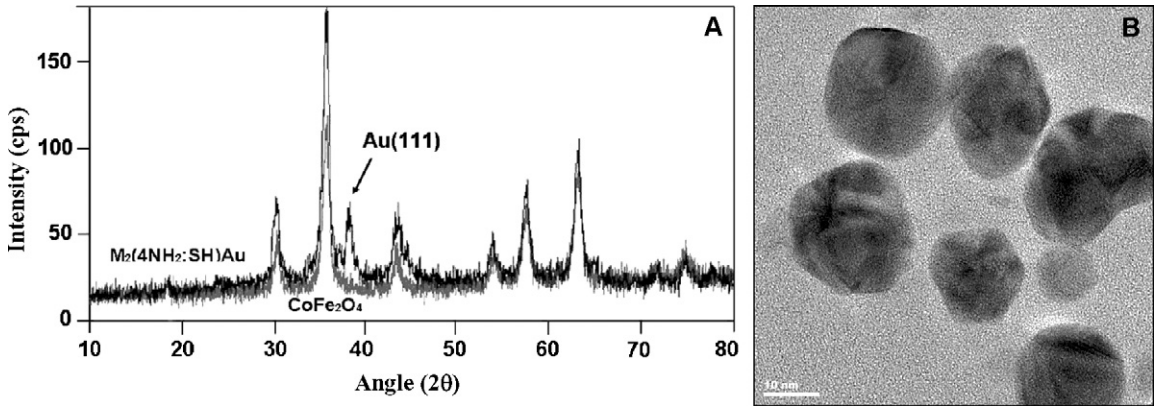

Fig. 5. (A) Comparison of XRD diffractograms for $CoFe_2O_4$ before and after gold covering. The appearance of Au(1,1,1) planar diffraction can be observed at 38 degrees. (B) Gold-covered magnetic nanoparticles, with diameter around 25 nm.

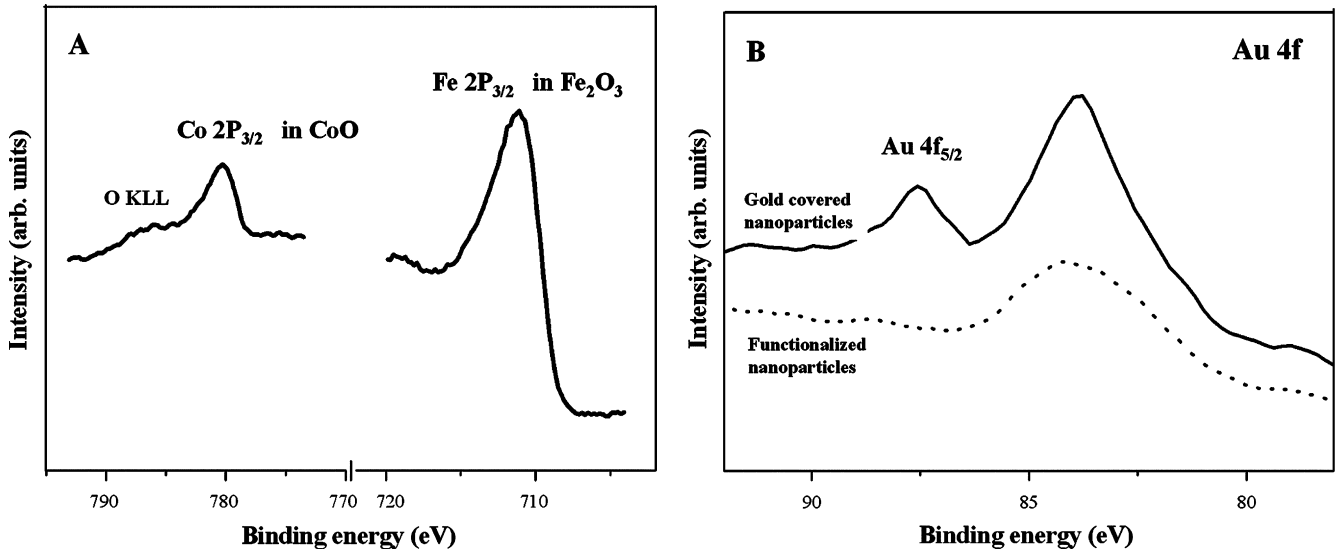

Fig. 6. (A) XPS core-level peaks of Co $3p_{3/2}$ and Fe $2p_{3/2}$ from the ($CoFe_2O_4$) magnetic core. The binding energies of these peaks are unaltered during the synthesis process. (B) Au $4f_{5/2}$ core-level peak from the gold-covered nanoparticle (upper curve) and the $M_2(4NH_2–SH)$ nanoparticles (lower curve). The peak at 84 eV in both curves corresponds to the Br 3d from the pellet.

molecules for the development of improved biosensors for genotyping applications. We were interested in the immobilization of PNA, an artificial molecule that is analogous to natural nucleic acids (DNA and RNA) and is capable of interacting with them through hydrogen-bonding between complementary nucleic bases [29,30]. The thiol-modified ssPNA immobilization on gold was previously optimized on planar metallic surfaces where the biomolecules formed ordered SAMs as measured by XPS, atomic force microscopy (AFM) and infrared spectroscopy (FTIR) [20,31]. This knowledge was used to immobilize PNA on the gold-covered nanoparticles, yielding a biosensor composite material that can be used to detect target DNA molecules complementary to the immobilized PNA probe. The immobilization of ssPNA on the nanoparticles have been characterized by FTIR spectroscopy (Supporting information, Fig. S2).

Hybridization experiments were performed by incubation of PNA-modified nanoparticles with a ssDNA oligomer containing the fully complementary sequence (5′-ATCCGGGGATT-3′) (HIBR) or with an oligomer showing a single mismatch (SMM) (5′-ATCCGAGGATT-3′) in the central nucleotide (Scheme 2). Evidence of hybridization was obtained by using Rhodamine 6G (Rh-6G) as a fluorescent dye marker. This molecule is able to bind hybridized DNA–PNA by electrostatic interactions with ssDNA through the negatively charged deoxyribose–phosphate backbone or via intercalation thus providing clear evidence of PNA–DNA hybridization. Since the PNA–DNA melting temperature (Tm) is decreased when a SMM is present, it should be possible to discriminate a SMM DNA probe from the HIBR probe by washing at a specific temperature. Therefore washing incubation steps were performed at 45, 45.5, 46 and 47 °C temperatures respectively to achieve binding specificity.

Fig. 7 depicts fluorescence emission spectra of Rh-6G retained by hybridized DNA–PNA-modified nanoparticles and PNA modified nanoparticles. At a washing temperature of 45 °C, both SMM and complementary DNA remain attached to the PNA on the nanoparticles (Fig. 7A).

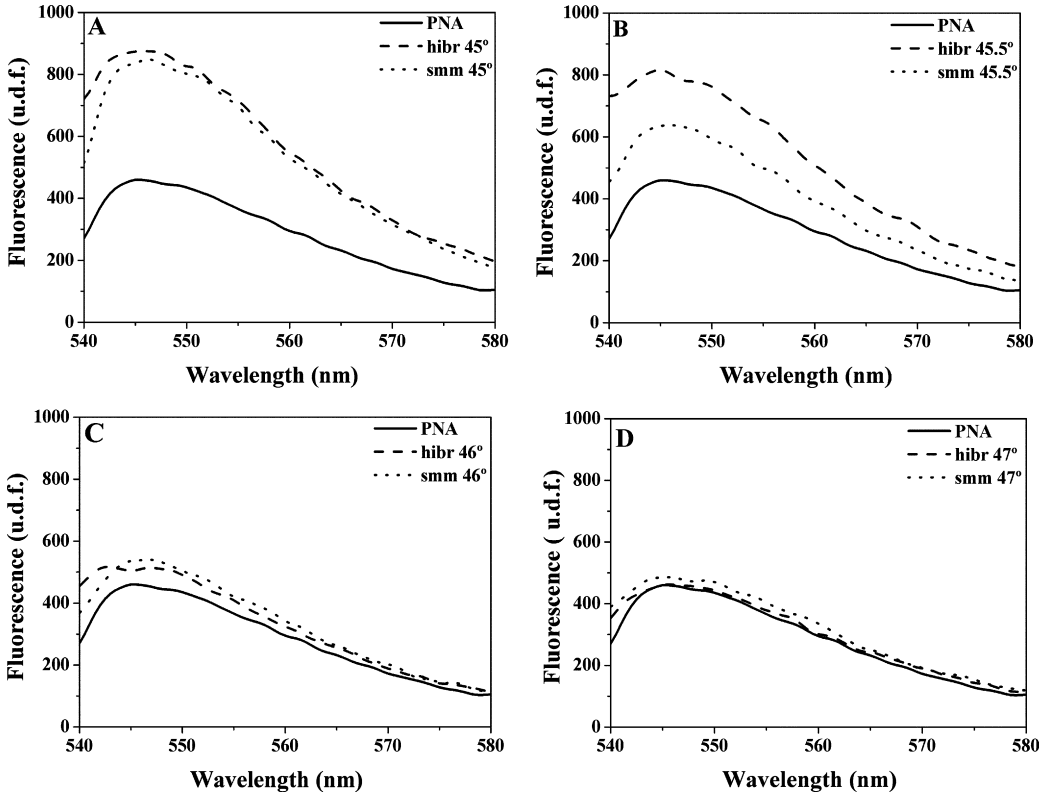

Fig. 7. Fluorescence showed by the Rhodamine 6G retained by the PNA–DNA heterodimmer when running the experiment with a complementary sequence and a single mismatch oligonucleotide. The hybridization temperature was 40 °C in all cases. The washing temperature was 45 °C (A), 45.5 °C (B), 46 °C (C) and 47 °C (D).

Optimal target-probe specificity is obtained at 45.5 °C as the fully complementary DNA target is retained, whereas DNA with a single mismatch is efficiently removed (Fig. 7B). At a temperature equal or higher than 46 °C both DNAs are melted and washed away from the particles (Fig. 7C). At 47 °C the fluorescent emission is practically equal to the non-DNA modified nanoparticles (Fig. 7D).

These results demonstrate that PNA-modified nanoparticles are able to bind present DNA probes in solution besides to the detection of a single nucleotide mutation in a short DNA sequence (only 11 nucleotides) avoiding time-consuming commonly procedures employed such as incubation or amplification by polymerase chain reaction.

Further improvements of the method developed here will include the use of natural double stranded (ds) DNA molecules as target material, as well as the optimization of experimental systems for the detection of DNA hybridization that avoid the use of fluorescent labels.

4. Conclusions

A gold-covered magnetic nanoparticles synthesis strategy is presented in this work, where the achievement of the gold shell is clearly improved by the use of a mixed amino-thiol functionalization. This composite nano-material is a versatile platform for immobilization of biomolecules. This can be used as an improved biosensor able to detect point mutations or single nucleotide polymorphisms (SNPs) in DNA by the modification of the gold surface with a suitable thiolated PNA, a relevant issue in the fields of genomics and molecular biology. Furthermore, the magnetic feature facilitates an easy separation and concentration after every reaction step avoiding traditional time-consuming separation procedures.

Acknowledgments

This work has been funded by the Programa Intramural of CSIC (Ref. 200450F0340). M.P. thanks the Consejería de Educación de la Comunidad de Madrid (CM), and the European Social Funding (F.S.E.) for the fellowship. J.M.A. acknowledges a postdoctoral fellowship from Fundación Ramón Areces. C.V. thanks the FPU program of the Science and Education Ministry for the fellowship. Work carried out at CAB was supported by EU, INTA, MEC and CM. We also wish to thank Ph.D. Student Alejandro Roca Gómez for acquiring the magnetite TEM picture.

Supporting information

The online version of this article contains additional supporting information.

Please visit DOI: 10.1016/j.jcis.2008.02.010.

References

[1] E. Katz, I. Willner, Angew. Chem. Int. Ed. 43 (2004) 6042.

[2] (a) E. Katz, Y. Weizzman, I. Willner, J. Am. Chem. Soc. 127 (2005) 9191; (b) J. Wang, Anal. Chim. Acta 500 (2003) 247.
[3] O. Bomati-Miguel, M.P. Morales, P. Tartaj, J. Ruiz-Cabello, P. Bonville, M. Santos, X.Q. Zhao, S. Veintemillas-Verdaguer, Biomaterials 26 (2005) 5695.
[4] A. Jordan, R. Scholz, P. Wust, H. Fahling, R. Felix, J. Magn. Magn. Mater. 201 (1999) 413.
[5] P. Tartaj, M.P. Morales, S. Veintemillas-Verdaguer, T. Gonzalez-Carreno, C.J. Serna, J. Phys. D Appl. Phys. 36 (2003) r182.
[6] Z.H. Ban, Y.A. Barnakov, V.O. Golub, C.J. O'Connor, J. Mater. Chem. 15 (2005) 4660.
[7] J. Lin, W.L. Zhou, A. Kumbhar, J. Wiemann, J.Y. Fang, E.E. Carpenter, C.J. O'Connor, J. Solid State Chem. 159 (2001) 26.
[8] J.M. Bai, J.P. Wang, Appl. Phys. Lett. 87 (2005) 152502.
[9] J.M. Abad, S.F.L. Mertens, M. Pita, V.M. Fernandez, D. Schiffrin, J. Am. Chem. Soc. 127 (2005) 5689.
[10] D. Caruntu, B.L. Cushing, G. Caruntu, C.J. O'Connor, J. Chem. Mater. 17 (2005) 3398.
[11] B.L. Oliva, A. Pradhan, D. Caruntu, C.J. O'Connor, M.A. Tarr, J. Mater. Res. 21 (2006) 1312.
[12] L.Y. Wang, J. Luo, M.M. Maye, Q. Fan, R.D. Qiang, M.H. Engelhard, C.M. Wang, Y.H. Lin, C.J. Zhong, J. Mater. Chem. 15 (2005) 1821.
[13] H. Yu, M. Chen, P.M. Rice, S.X. Wang, R.L. White, S.H. Sun, Nano Lett. 5 (2005) 379.
[14] G. Jeong, T.H. Ta, B.H. Chung, Anal. Chim. Acta 569 (2006) 203.
[15] G.K. Kouassi, J. Irudayaraj, Anal. Chem. 78 (2006) 3234.
[16] M. Mandal, S. Kundu, S.K. Ghosh, S. Panigrahi, T.K. Sau, S.M. Yusuf, T. Pal, J. Colloid Interface Sci. 286 (2005) 187.
[17] V. Salgueirino-Maceira, M.A. Correa-Duarte, M. Farle, A. Lopez-Quintela, K. Sieradzki, R. Diaz, Chem. Mater. 18 (2006) 2701.
[18] T. Pellegrino, S. Kudera, T. Liedl, A.M. Javier, L. Manna, W.J. Parak, Small 1 (2005) 48.
[19] K.R. Brown, D.G. Walter, J. Natan, Chem. Mater. 12 (2000) 306.
[20] (a) C. Briones, E. Mateo-Marti, C. Gomez-Navarro, V. Parro, E. Roman, J.A. Martin-Gago, Phys. Rev. Lett. 93 (2004) 208103;
(b) C. Briones, E. Mateo-Marti, C. Gomez-Navarro, E. Roman, V. Parro, J.A. Martin-Gago, J. Mol. Catal. A Chem. 228 (2005) 131.
[21] S.N. Letuta, G.A. Ketsle, L.V. Levshin, A.N. Nikiyan, O.K. Davydova, Opt. Spectrosc. 93 (2002) 844.
[22] J. Wagner, T. Autenrieth, R. Hempelmann, J. Magn. Magn. Mater. 252 (2002) 4.
[23] R. Massart, IEEE Trans. Magn. 17 (1981) 1247.
[24] V.M. Fernandez, J.A. Martin-Gago, M. Pita, J.C. Serna, C. Vaz, C. Briones, E. Mateo-Marti, World patent application WO/2007/034021 and PTC application PTC/ES2006/070134.
[25] (a) D.G. Duff, A. Baiker, P.P. Edwards, Langmuir 9 (1993) 2301;
(b) D.G. Duff, A. Baiker, I. Gameson, P.P. Edwards, Langmuir 9 (1993) 2310.
[26] J.L. Lyon, D.A. Fleming, M.B. Stone, P. Schiffer, M.E. Williams, Nano Lett. 4 (2004) 719.
[27] P. Klug, L.E. Alexander, X-Ray Diffraction Procedure, Wiley, New York, 1954, Chapter 9.
[28] J.P. Wilcoxon, J.E. Martin, P. Provencio, Langmuir 16 (2000) 9912.
[29] (a) P.E. Nielsen, M. Egholm, R.H. Berg, O. Buchardt, Science 254 (1991) 1497;
(b) M. Egholm, O. Buchardt, P.E. Nielsen, R.H. Berg, J. Am. Chem. Soc. 114 (1992) 1895;
(c) V. Menchise, G. de Simone, T. Tedeschi, R. Corradini, S. Sforza, R. Marchelli, D. Capasso, M. Saviano, C. Pedone, Proc. Natl. Acad. Sci. 100 (2003) 12021.
[30] C. Briones, J.A. Martín-Gago, Curr. Nanosci. 2 (2006) 257.
[31] E. Mateo-Martí, C. Briones, E. Román, E. Briand, C.M. Pradier, J.A. Martín-Gago, Langmuir 21 (2005) 9510.